

# Estimating iceberg melt rates from video using novel view synthesis

Zhao Xiaohui<sup>\*†</sup>, Hari Vishnu<sup>\*</sup>, Mandar Chitre<sup>\*†</sup>, Bharath Kalyan<sup>\*</sup>,  
Hayden Johnson<sup>+</sup>, Oskar Glowacki<sup>‡</sup>, Dale Stokes<sup>+</sup>

<sup>\*</sup>Acoustic Research Laboratory, Tropical Marine Science Institute, National University of Singapore

<sup>†</sup>Department of Electrical and Computer Engineering, National University of Singapore

<sup>+</sup>Scripps Institution of Oceanography, University of California, San Diego

<sup>‡</sup>Institute of Geophysics, Polish Academy of Sciences

**Abstract**—Understanding iceberg melt is crucial for assessing climate change effects in polar regions. This paper investigates the geometric reconstruction and volume estimation of icebergs using multi-view imagery, combining Structure-from-Motion (SfM) and Neural Radiance Fields (NeRFs). High-resolution multi-view datasets are processed through SfM techniques to estimate camera poses, which are subsequently used to generate a 3D model of the object using NeRF. The proposed framework successfully reconstructs iceberg geometry and estimates its volume, ultimately providing estimates of melting rates. This study demonstrates the possibility of applying SfM and NeRFs for monitoring iceberg dynamics, offering a new approach to analyzing iceberg volume and volume flux.

**Index Terms**—3D model, computer vision, iceberg, Arctic, climate change, neural radiance field, structure from motion

## I. INTRODUCTION

In tidewater glacial bays, calving and submarine-melting account for most of the ice loss via frontal ablation. Calving generates floating ice in the bay in the form of ice-mélange, icebergs and bergy-bits. Iceberg melting has complex feedback effects on the global climate system and marine ecosystems [1]–[3]. The freshwater from melting icebergs contributes to freshwater fluxes and alters seawater salinity, potentially affecting ocean properties and mechanisms, such as the Atlantic meridional overturning circulation and sea level [4]–[6]. These oceanic changes redistribute heat, influence the carbon cycle, and affect the global climate. Additionally, melting icebergs also impact local flora and fauna habitats in terms of physical and biological parameters, consequently affecting entire ecosystems [3], [7]–[9].

Various approaches have been proposed to calculate iceberg melting rates. Simulations have been used to model environmental factors affecting iceberg melting, with controlled variables such as water flow velocity, water temperature, salinity, forced convection conditions, and iceberg shape [10]–[13]. Though these laboratory studies simulate real-world conditions as closely as possible, they primarily explore the influencing factors and the approximate magnitude of their effects, making it challenging to accurately apply them in the real-world environment. Acoustic [14] and direct techniques [15] are also being studied for in-situ iceberg melt estimation.

With advances in artificial intelligence, direct approaches to calculating iceberg melting rates using Synthetic Aperture



Fig. 1: Locations in Svalbard where field campaigns were undertaken - Hornsund fjord and Kongsfjorden (marked by yellow stars).

Radar (SAR) and aerial photogrammetry combined with GPS iceberg geometry reconstruction [16]–[18] are being explored. SAR is regularly and effectively used to measure the surface area covered by ice sheets, but may struggle to detect small icebergs, particularly against the ocean background [18].

Compared to SAR, multi-view images captured by cameras can capture the complete geometric shape of icebergs, allowing for surface reconstruction and direct measurement of their above-water size reduction over time [19]. These images also capture iceberg surface texture and morphology. SfM techniques can use these images to recover camera poses and a sparse 3D structure of the scene, while multi-view stereo algorithms can generate a dense point cloud, enhancing the model’s detail and accuracy. Various commercial software

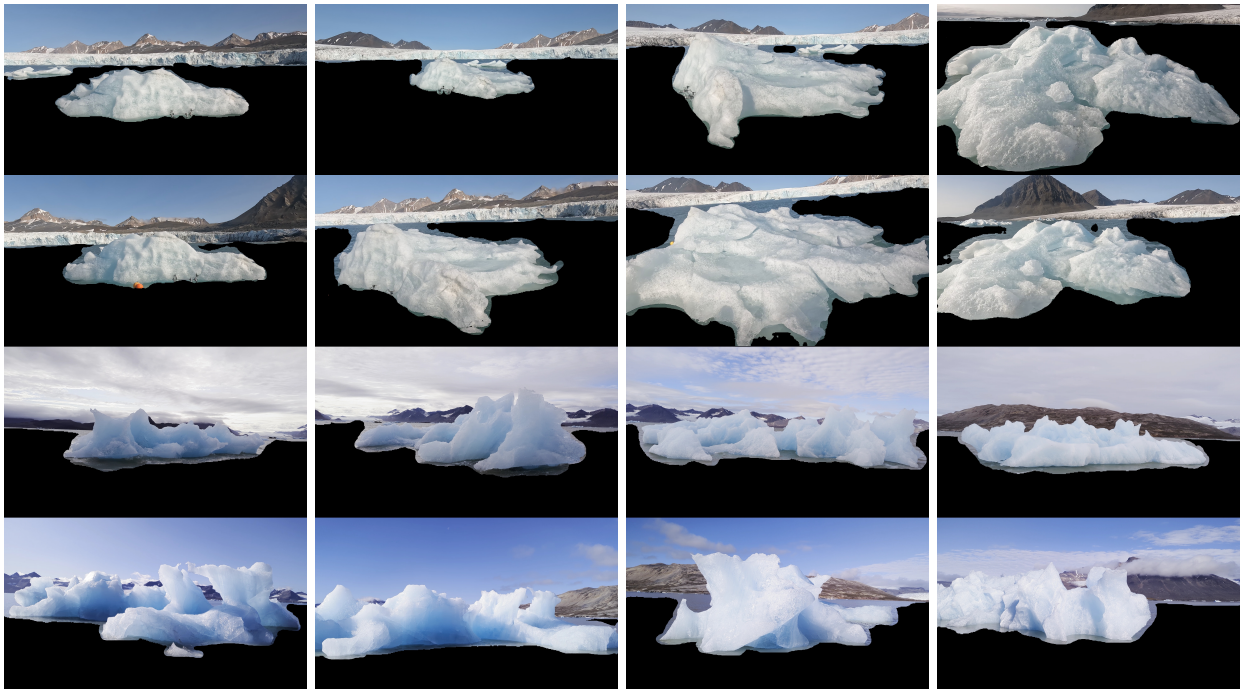


Fig. 2: Iceberg images from the four videos (rows 1-4) after frame extraction, resizing, and masking.

tools such as COLMAP [20], combine these steps to automate surface reconstruction and have been widely applied to fields like coral reef [21], river reach studies [22], and forest canopy analysis [23].

In 2021, a 3D novel-view-synthesis method called NeRF [24] was proposed, using neural networks to simulate and render volume density and color distribution in scenes from a series of 2D images. The advantage of this is that (1) it does not require active imaging techniques like LIDAR, and can be done even with simple phone-based cameras in the field, which are less bulky, inexpensive and easily available, (2) it is non-invasive, and does not add any pollutant into the environment. This algorithm has been applied to 3D reconstruction for fields as varied as cultural heritage artefacts and scenes [25], [26] and analysis of damage in aviation [27]. Compared to traditional multi-view stereo, NeRF performs better in reconstructing texture-less and reflective surfaces [28] such as those of icebergs.

Field campaigns were undertaken in 2023 in Svalbard to record visual and acoustic data near the glacier termini. During these campaigns, we collected videographic survey data of icebergs at different time-points, during which the icebergs melt a certain amount. This paper presents the reconstruction of geometries and the estimation of above-water volume of these icebergs using this video data. Based on these data, the difference in iceberg volume, and thus meltwater volume flux during the duration between which the videos were acquired, can be estimated.

In Section II, we describe the dataset used in this study. Section III outlines the methodology including the camera pose estimation and NeRF reconstruction technique, including

a detailed parametric study and discussion of the effective processing chain. The melt-rate estimation results are presented in section IV. Finally, section V summarizes and concludes the paper.

## II. DATA COLLECTION

We undertook field campaigns in two regions in Svalbard – (1) Hornsund fjord and (2) Kongsfjorden, shown in Fig. 1, to conduct in-situ melting studies and passive acoustics, visual data, active acoustics, and robot-based surveys near the glacier termini [14], [29], [30]. The Hornsund campaign was staged from the Polish Polar Research station, and the Kongsfjorden campaign was staged from the Norwegian Polar Institute research station in Ny-Ålesund. The video data used here consists of:

- 1) Dataset 1: Two videos captured using a handheld GoPro 10 camera from a boat while it was driven around an iceberg named #1 at Hornsund fjord, on July 24, 2023 at 14:25 hrs and 15:18 hrs UTC, and
- 2) Dataset 2: Two videos shot with an Android phone around an iceberg (named #2) in Kongsfjorden along with GPS data recorded every second, filmed on 7th August 2023 at 6:27 hrs and 9:15 hrs UTC.

In both cases, the water depth was determined to be large enough that the iceberg was floating. Video footage in Hornsund was acquired by driving the Polish station’s Zodiac boat to a spot within safe distance from the glacier terminus, and surveying an iceberg in the bay. Footage in Kongsfjorden was acquired by using a Polarcirkel boat from the Norwegian Polar Institute station to drive out to Kongsfjorden and surveying icebergs.

	# Features with SIFT	# Features with DSP-SIFT
Dataset 1, video #1	1508881	1394973
Dataset 1, video #2	1860827	1696885
Dataset 2, video #1	1165122	1079960
Dataset 2, video #2	1912056	1760838

TABLE I: Number of feature points obtained for each video using the two approaches of SIFT based feature extraction.

### III. METHODOLOGY

In recent years, deep learning-based algorithms have emerged as the dominant method for generating 3D scenes from 2D images without requiring knowledge of its 3D structural ground truth. One of the emerging techniques is NeRF [24] which maps each point and view information in 3D space into the corresponding color and density values, so that images from different viewpoints can be synthesized. This method learns the scene by training a neural network model, and uses volume rendering techniques to convert this information into realistic images with details and features captured accurately.

The basic methodology used in this paper is to apply NeRF to reconstruct the 3D volume of icebergs exposed above the water surface. The steps involved in this include

- 1) Collecting the videos collected from the scene surveying each iceberg in two separate runs, converting them into photo frames, and downsampling or downsizing them.
- 2) Estimating the camera pose for each of the photos using COLMAP SfM [20], [31], within an artificial reference frame defined for each video by the software.
- 3) Building a 3D reconstruction of the scene from the estimated camera poses using NeRF.
- 4) Exporting the reconstruction into a mesh form where it can be edited and post-processed further.
- 5) Post processing and repairing the mesh.
- 6) Estimating volume of the iceberg object in the COLMAP reference frame.
- 7) Estimating the scaling relating the real-world size to the COLMAP reference frame.
- 8) Comparing iceberg volumes from the two runs and estimating the volume flux.

In the following sections, these steps will be detailed.

#### A. Dataset preprocessing

Video datasets acquired from each location are converted into a set of individual frames, which can be treated as if captured by multi-view cameras with consistent intrinsic parameters, assuming the scene is quasi-static. The frame rate and resolution of the cameras are higher than required for the current problem, yielding too many images which makes pose estimation and 3D reconstruction computationally expensive and infeasible. Thus, the video frames are down-sampled, preserving just enough information for accurate 3D reconstruction. The first video is downsampled in time by a factor of 14, and resized from  $3840 \times 2176$  to  $1920 \times 1088$ . The second video’s frames are downsized by a factor of 15. The initial resolution of the second video is  $1920 \times 1088$ , and no resizing was done.

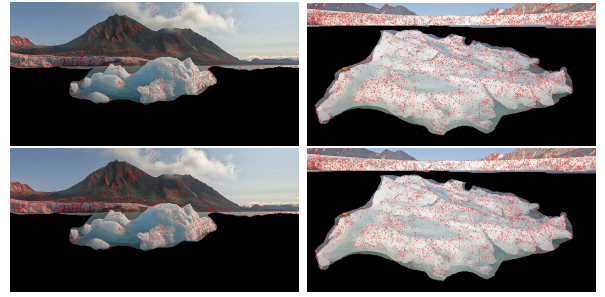


Fig. 3: Feature extraction results: SIFT (top rows) and DSP-SIFT with affine shape estimation (bottom rows) - the location points of the features are marked as red dots.

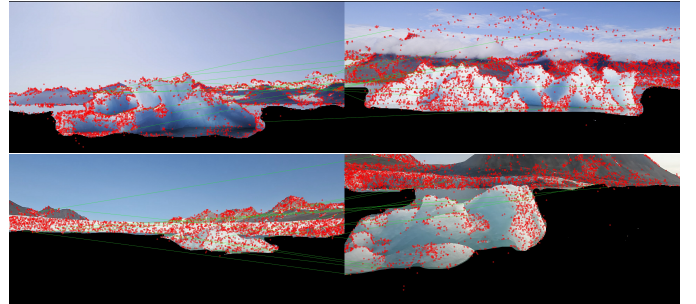


Fig. 4: Incorrect feature matching results with SIFT’s feature points.

#### B. Camera Pose estimation

SfM is a computer vision technique used to reconstruct 3D structures from a series of 2D images taken from different viewpoints. SfM estimates camera positions and creates a sparse 3D point cloud of the observed scene. COLMAP [20], [31] is an SfM software that pairs all images together and measure the cosine similarity of each feature point descriptor to determine whether they are the same point in the 3D world. We utilize COLMAP for the camera pose estimation prior to NeRF - this involves feature extraction, feature matching, and sparse reconstruction steps. Although the ground truth of the camera pose is unavailable, we evaluate the quality of the estimated poses by assessing their consistency, comparing them with GPS data (for dataset 2), and qualitatively analyzing the quality of the resulting 3D reconstructions. These methods help guide adjustments to the parameters used in the estimation process.

COLMAP allows the use of masks to define which regions to ignore or include when generating camera pose estimates from the images. We use the segmentation software Sefexa to mask out the sea surface pixels in each frame, retaining only the iceberg and background in each image. This is because we find that the background, which is static and more feature-rich, plays a crucial role in providing enough features for estimating camera poses. The water surface was not quasi-static due to changing sea surface-waves in each frame, which interferes with the pose estimation, so the sea water has to be masked. This will be discussed more under point (2) below. We

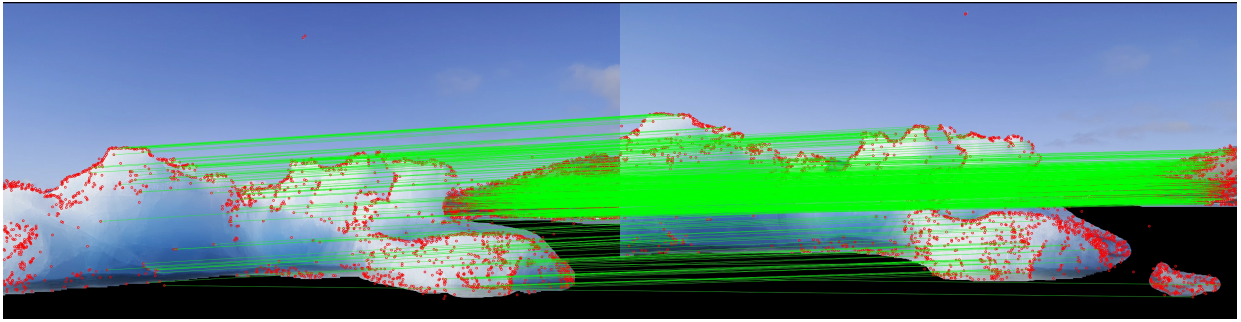


Fig. 5: Feature matching results using default parameters in COLMAP, with an example pair of images. The matches are shown in the form of the green lines connecting the corresponding red dots in the two images.

also manually remove images that were far from the iceberg because these contribute too little information and add to the computational complexity.

Now, we discuss each step, and compare the selection of different parameters in COLMAP to obtain good pose estimates.

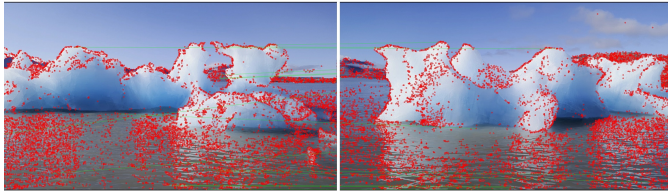


Fig. 6: Mismatch between water surface and iceberg features.

1) *Feature extraction*: In Table I, we compare the total number of feature points obtained by the feature matching algorithm using a (i) standard shift-invariant feature transform (SIFT) algorithm and (ii) domain-size pooled (DSP)-SIFT with affine shape estimation. Using DSP-SIFT with estimating affine shape, the total number of feature points has decreased because affine shape estimation introduces more constraints for extracting feature points. However, after DSP-SIFT feature extraction, the number of feature points on the glacier has increased and the number of unstable feature points along the mountains' boundary has decreased slightly as shown in Fig. 3. Furthermore, results from the feature matching stage (discussed next) further proves the better stability of using DSP-SIFT with affine shape estimation. SIFT produces a significant number of false matches as shown in Fig. 4 which DSP-SIFT does not. Hence, moving forward, we will use DSP-SIFT with affine shape estimation in the feature extraction step.

2) *Feature matching*: Matching results using default COLMAP parameters are shown in Fig. 5. Some of the good matched pairs appear in the background, which shows the importance of the background for achieving effective matching. One of the reasons for this is that there are not enough sharp and distinct features on the iceberg itself for matching, whereas the background has richer and unambiguous features that enable good matching. This is why we retain the background

in the mask during the feature extraction stage. The sea water features, on the other hand, are noisy because (1) the color of seawater does not change over different regions and in different poses and (2) the surface waves keep changing from frame-to-frame, removing the consistency needed to estimate poses correctly. As shown in Fig. 6, sea surface features are very weak under different light and shadow conditions and there are some mismatch between sea surface features and iceberg features. This is the reason why we mask the sea surface part out.

Another important parameter to be fine-tuned is the confidence level used for matching. If the level is set too high, fewer points will be matched. Conversely, if it is too low, more inaccurate points may be matched and hence the overall matching results may become inaccurate. Both situations can negatively impact the subsequent estimation, so we need to find the sweet-spot in terms of this parameter.

For dataset 1, a confidence level of 0.993 yields the most continuous camera poses, with no noticeable gaps between frames. In dataset 2, when the level exceeds 0.992, the camera poses remain continuous, and increasing the level further does not improve performance. However, a closer look at the 3D reconstructed mesh reveals that while the performance difference between using levels of 0.992 and 0.993 is minor, the mesh volume generated is inconsistent between the two. While this does not necessarily have a bearing on the quality of the feature matching, it shows the importance of maintaining a consistent confidence level within the same dataset to ensure uniformity in the resulting mesh volumes. Based on this, we decide to set the matching confidence level of the two videos in dataset 1 to 0.993, while that of the two videos in dataset 2 is set at 0.992. The camera pose estimates are shown in Fig. 7, and the corresponding mesh generated in Fig. 8.

3) *Camera pose estimation*: First, images where the iceberg is far away are removed because they lead to errors in the final camera pose estimation. The pose estimates and sparse reconstruction of iceberg 1 are shown in Fig. 9. Reconstructions from both videos show good consistency as assessed in COLMAP.

For dataset 2, apart from assessing the consistency of the camera poses, the estimated camera trajectory is compared

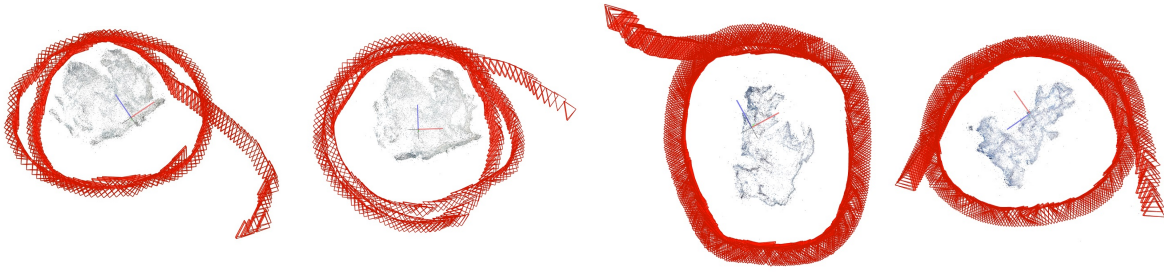


Fig. 7: Camera pose estimates using feature matching with confidence level 0.993. The grey point cloud in the center is the sparse reconstruction of the iceberg, and the surrounding red triangles show the pose estimates.

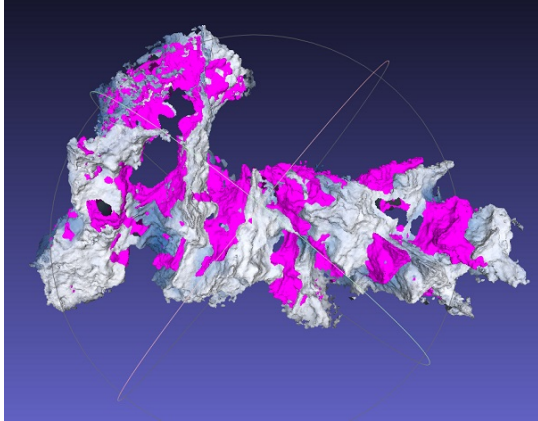


Fig. 8: Mesh generated using 0.993 confidence level in feature matching.

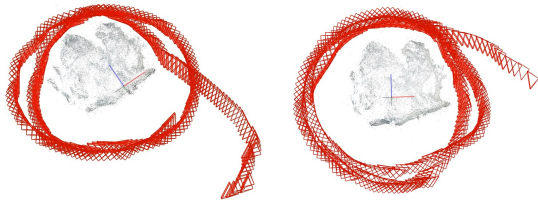


Fig. 9: Camera pose estimates for dataset 1.

with the movement trajectory indicated via GPS to verify the performance. As shown in Fig. 10, the estimated trajectory is very close to the GPS-based trajectory, validating the estimated poses. There is a slight mismatch in the trajectories in one section. By visual comparison of the images at this point of

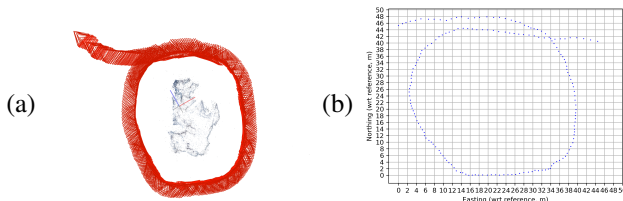


Fig. 10: (a) Camera pose estimates and (b) GPS track of dataset 2.

mismatch, we conclude that the COLMAP estimates seem more accurate for these images, and the inconsistency is likely due to slight errors in the GPS data.

### C. 3D reconstruction result evaluation

1) *NeRF reconstruction result*: The rendering quality of the reconstruction is usually measured using three quality indicators, namely (i) Peak Signal to Noise Ratio (PSNR), (ii) Structural Similarity (SSIM) [32] and (iii) Learned Perceptual Image Patch Similarity (LPIPS) [33]. These are mainly used to measure the similarity between the real image and the corresponding image synthesized by NeRF. PSNR measures the pixel-level differences between images, with higher values indicating more similar images, while SSIM measures the structural similarity of the images. The closer the SSIM is to 1, the more similar the images are in terms of feature structure. LPIPS detects image differences through deep networks, and smaller values indicate more similar images.

	PSNR	SSIM	LPIPS
Dataset 1, run #1	21.26	0.76	0.316
Dataset 1, run #2	20.47	0.758	0.31
Dataset 2, run #1	18.13	0.85	0.307
Dataset 2, run #2	19.05	0.838	0.297

TABLE II: Evaluation metrics of NeRF rendering output.

The three metrics evaluated for the NeRF reconstructions are tabulated in table II and the rendering results are shown in Fig. 11. The metrics indicate the rendering results are of reasonable quality to proceed with the objective in this work. By comparing with the original frame in Fig. 2, we find that all the details of the iceberg surface are well reconstructed. This demonstrates that NeRF rendering performs effectively from various viewing angles and that the overall 3D reconstruction of the scene is of high quality. There are some inaccuracies such as black points visible in the sky - however, these are an artefact of the masks used in the images, and inconsequential to our problem.

The NeRF 3D reconstruction is exported into a mesh form, shown in Fig. 12. For each mesh, we remove the black parts (artefacts of the masks used) and isolated pieces in the mesh with a radius smaller than 0.08 pixel units in MeshLab. Most of the iceberg details are preserved. However, some holes are observed at the top of the mesh for dataset 2, because the

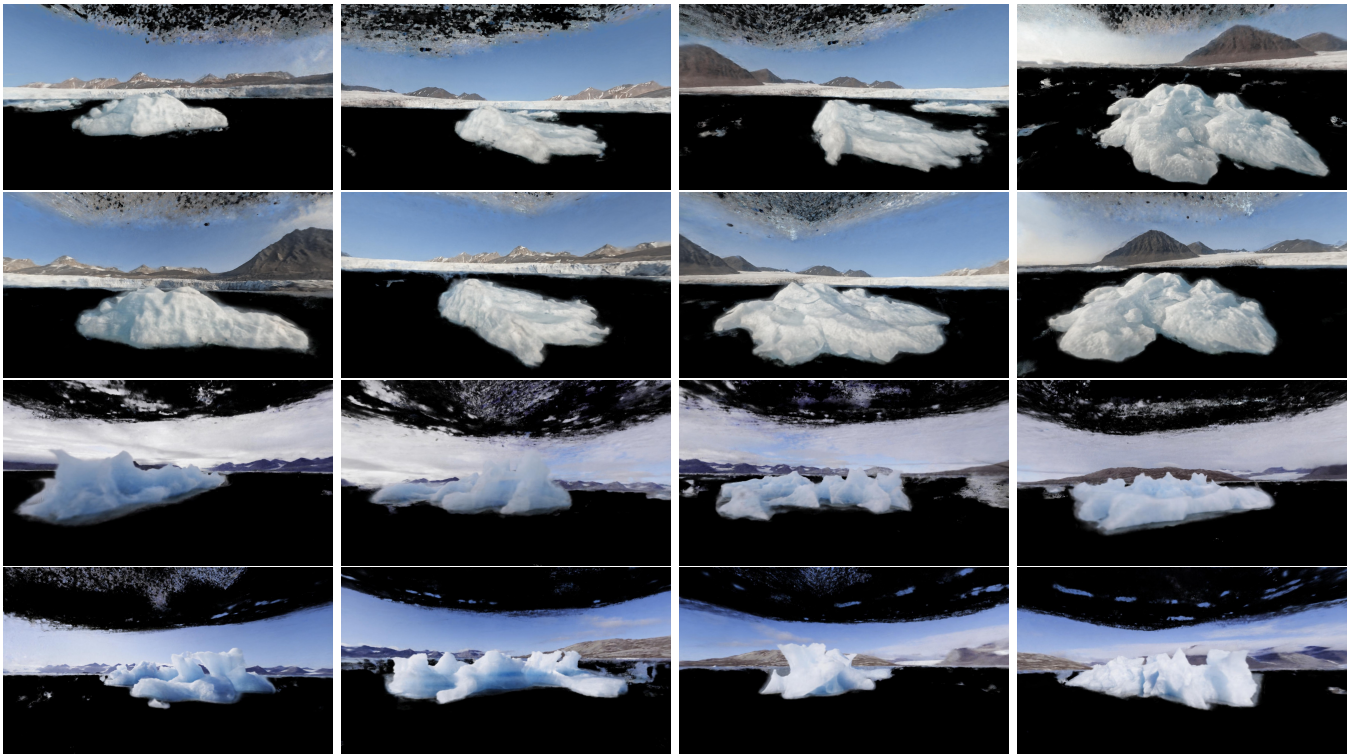


Fig. 11: NeRF rendering results.

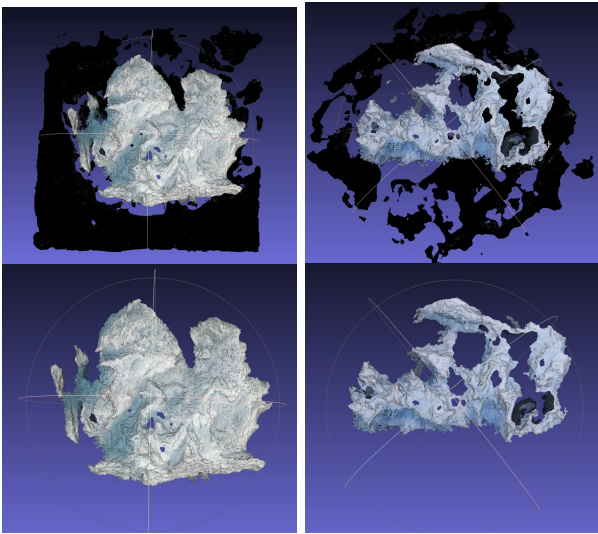


Fig. 12: Two example top views of exported mesh before repairing (top row) and after repairing (bottom row).

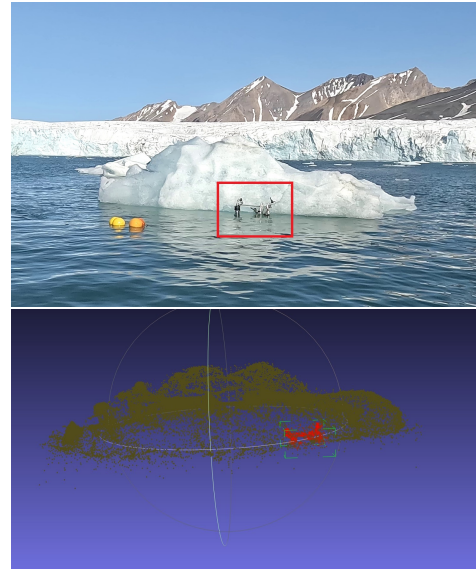


Fig. 13: The object of known dimensions in the real scene, described in [15], and the point cloud exported after NeRF reconstruction.

captured images are taken at eye-level and cannot provide any color and density information at these locations for NeRF to train, so the NeRF assumes these parts of the iceberg are empty, or ‘hollow’. After this, we convert the mesh into a solid object, fill the holes on the upper surfaces and the missing bottom surface, and calculate its volume.

#### IV. SCALE RECOVERY AND MELTING RATE ESTIMATION

For dataset 1, based on the known camera model and parameters, the scaling factor is calculated to be 6.17 m/pixel and 4.55 m/pixel for horizontal and vertical scaling respectively. We also verify this based on an object of known dimensions

that was present in the scene as shown in Fig. 13 - the scale factor estimated based on the dimensions of this object matched the scaling calculated for the camera model.

Iceberg 1's volume is thus estimated as  $V_1 = 3.05 \text{ m}^3$  and  $V_2 = 2.67 \text{ m}^3$  in the first and second videos respectively. The volume reduction in the surface-exposed part of iceberg 1 is estimated as  $0.43 \text{ m}^3/\text{hour}$ .

For a floating iceberg with a given density (assumed  $902.5 \text{ kg/m}^3$  for fresh glacier ice), the submerged ice fraction is equal to the ice density relative to sea water, estimated as 0.879. Therefore, the absolute melt rate across the total iceberg volume can be estimated as  $\frac{0.43}{1-0.879} = 3.55 \text{ m}^3/\text{hour}$ . The melt rate relative to the initial volume for iceberg 1 is estimated as  $\frac{V_1-V_2}{V_1 \times 0.88} = 14.2 \text{ \%}/\text{hour}$ .

For dataset 2, the camera's parameters are not known for us to be able to calculate the scale directly. However, we can estimate the scale from the GPS data by comparing the distances of the camera tracks in COLMAP with those in the GPS data. Although there are small errors in the GPS data, they are within acceptable margins for the sake of this problem because the track span is large enough.

Iceberg 2's volume in the first and second videos is estimated as  $V_3 = 1.15 \text{ m}^3$  and  $V_4 = 0.58 \text{ m}^3$  respectively. The reduction in volume of the surface-exposed portion for iceberg 2 is estimated as  $0.2 \text{ m}^3/\text{hour}$ . Thus, the absolute melt rate across the total iceberg volume is estimated as  $1.653 \text{ m}^3/\text{hour}$ . The melt rate relative to initial volume is estimated as  $\frac{V_3-V_4}{V_3 \times 2.8} = 18\% /\text{hour}$  for iceberg 2.

## V. CONCLUSION

In this study, we used NeRF combined with SfM to successfully reconstruct the 3D geometry of the above-water portion of two icebergs from video acquired with hand-held cameras. Thereby, we demonstrated the feasibility of accurately reconstructing complex iceberg shapes and surfaces and estimating meltwater volume flux, and validated NeRF's performance in handling ice surfaces with less color diversity and reflectiveness. The technique developed herein is shown to perform well on the aerial imagery data acquired from the field.

The advantage of this technique is that (1) it does not require active imaging techniques like LIDAR for volume estimation, and can be done even with simple phone-based cameras in the field, which are less bulky, inexpensive and easily available, (2) it is non-invasive. Its drawback is that it can only directly estimate the volume (and melt-rate) based on the part of the iceberg above water - however, this can also be used to infer the overall melting of the iceberg by using assumptions on the density of the ice which allows us to estimate the volume of ice submerged (assuming the iceberg is floating, and not grounded). The experimental results indicate that the methodology can provide an easy way for iceberg volume estimation, making it a valuable tool for iceberg monitoring studies. This method also requires access to the region near the iceberg, and may be sensitive to visibility conditions. Careful acquisition of the iceberg video from sufficient viewing angles

is also necessary for good performance. This technique may also be used to estimate the retreat rate (in m/day units) of ice-boundaries (such as glacier termini) by estimating the real-world coordinates of the estimated 3D mesh, or that of 3D objects like icebergs by dividing the volume flux by the average surface area of the iceberg, but these have not been attempted in this work.

Some of the steps that helped improve the technique included

- Masking the sea surface pixels in the images prior to SfM,
- Using DSP-SIFT feature extraction with affine shape estimation,
- Parametric study on the confidence level which yielded the reconstruction of the best quality, and
- Weeding out images that were too far away to provide useful features.

Future research could focus on validating the volume estimates against estimates obtained from other techniques, to benchmark its accuracy.

## ACKNOWLEDGEMENTS

We acknowledge the funding support from the INTERACT III Transnational Access grant under the European Union H2020 Grant Agreement No.871120, and the Arctic Field grant Project No. 342135 under the Research Council of Norway, for the travel and logistics for the campaigns, and the National Science Centre, Poland (grant 2021/43/D/ST10/00616), and a subsidy for the Institute of Geophysics, Polish Academy of Sciences provided by the Ministry of Science and Higher Education of Poland. We thank the Polish Polar station, Hornsund, and the Norwegian University of Science and Technology for helping with administration of the funds, as well as facilities during the campaign. We also thank Kingsbay AS and the Norwegian Polar Institute research station at Ny-Ålesund for their facilities support. We are grateful to Grant Deane for discussions on iceberg melt-rate estimation, Too Yuen Min for discussion on NeRF, and Asgeir Sørensen, Halvar Gravråkmo and Rabea Rogge for support during the campaign at Kongsfjorden.

## REFERENCES

- [1] R. K. Haskins, K. I. Oliver, L. C. Jackson, R. A. Wood, and S. S. Dri-jfhout, "Temperature domination of amoc weakening due to freshwater hosing in two gems," *Climate Dynamics*, vol. 54, pp. 273–286, 2020.
- [2] P. Bakker, A. Schmittner, J. Lenaerts, A. Abe-Ouchi, D. Bi, M. van den Broeke, W.-L. Chan, A. Hu, R. Beadling, S. Marsland *et al.*, "Fate of the atlantic meridional overturning circulation: Strong decline under continued warming and greenland melting," *Geophysical Research Letters*, vol. 43, no. 23, pp. 12–252, 2016.
- [3] A. Jenkins and D. Holland, "Melting of floating ice and sea level rise," *Geophysical Research Letters*, vol. 34, no. 16, 2007.
- [4] O. Dangles, A. Rabatel, M. Kraemer, G. Zeballos, A. Soruco, D. Jacobsen, and F. Anthelme, "Ecosystem sentinels for climate change? evidence of wetland cover changes over the last 30 years in the tropical andes," *PloS one*, vol. 12, no. 5, p. e0175814, 2017.
- [5] R. Cazzolla Gatti, A. Dudko, A. Lim, A. I. Velichevskaya, I. V. Lushchaeva, A. V. Pivovarova, S. Ventura, E. Lumini, A. Berruti, and I. V. Volkov, "The last 50 years of climate-induced melting of the maliy aktru glacier (altai mountains, russia) revealed in a primary ecological succession," *Ecology and Evolution*, vol. 8, no. 15, pp. 7401–7420, 2018.

- [6] C. Cenedese and F. Straneo, "Icebergs melting," *Annual Review of Fluid Mechanics*, vol. 55, no. 1, pp. 377–402, 2023.
- [7] M. Bascur, C. Muñoz-Ramírez, A. Román-González, K. Sheen, D. K. Barnes, C. J. Sands, A. Brante, and Á. Urzúa, "The influence of glacial melt and retreat on the nutritional condition of the bivalve *Nuculana inaequisculpta* (protobranchia: Nuculanidae) in the west antarctic peninsula," *Plos One*, vol. 15, no. 5, p. e0233513, 2020.
- [8] J. Dinasquet, I. Richert, R. Logares, P. Yager, S. Bertilsson, and L. Riemann, "Mixing of water masses caused by a drifting iceberg affects bacterial activity, community composition and substrate utilization capability in the southern ocean," *Environmental Microbiology*, vol. 19, no. 6, pp. 2453–2467, 2017.
- [9] H. Vishnu, G. B. Deane, M. Chitre, O. Glowacki, D. Stokes, and M. Moskalik, "Vertical directionality and spatial coherence of the sound field in glacial bays in Hornsund Fjord," *The Journal of the Acoustical Society of America*, vol. 148, no. 6, pp. 3849–3862, dec 2020. [Online]. Available: <http://asa.scitation.org/doi/10.1121/10.0002868>
- [10] A. Marchenko and N. Marchenko, "Laboratory investigations of iceberg melting under wave conditions in sea water," *Journal of Marine Science and Engineering*, vol. 12, no. 3, p. 501, 2024.
- [11] J. Sweetman, C. Shakespeare, K. Stewart, and C. McConnochie, "Laboratory experiments of melting ice in warm salt-stratified environments," *Journal of Fluid Mechanics*, vol. 984, p. A42, 2024.
- [12] O. Shipilova, A. Olsson, and M. Thomson, "On the shape factor in iceberg deterioration by forced convection," *Cold Regions Science and Technology*, vol. 195, p. 103472, 2022.
- [13] S. Kimura, K. W. Nicholls, and E. Venables, "Estimation of ice shelf melt rate in the presence of a thermohaline staircase," *Journal of Physical Oceanography*, vol. 45, no. 1, pp. 133–148, 2015.
- [14] H. Johnson, G. Deane, O. Glowacki, D. Stokes, M. Chitre, H. Vishnu, and E. Weidner, "Acoustic observations of individual bubble release events from melting glacier ice in an arctic fjord," *The Journal of the Acoustical Society of America*, vol. 155, no. 3, pp. A99–A100, mar 2024.
- [15] H. A. Johnson, O. Glowacki, G. B. Deane, and M. D. Stokes, "Brief communication: A technique for making in situ measurements at the ice-water boundary of small pieces of floating glacier ice," *The Cryosphere*, vol. 18, no. 1, pp. 265–272, 2024.
- [16] M. M. Barbat and M. M. Mata, "Iceberg drift and melting rates in the northwestern weddell sea, antarctica: Novel automated regional estimates through machine learning," *Anais da Academia Brasileira de Ciências*, vol. 94, no. suppl 1, p. e20211586, 2022.
- [17] A. Crawford, G. Crocker, D. Mueller, L. Desjardins, R. Saper, and T. Carrieres, "The canadian ice island drift, deterioration and detection (ci2d3) database," *Journal of Glaciology*, vol. 64, no. 245, pp. 517–521, 2018.
- [18] M. M. Barbat, C. Wesche, A. V. Werhli, and M. M. Mata, "An adaptive machine learning approach to improve automatic iceberg detection from sar images," *ISPRS Journal of Photogrammetry and Remote Sensing*, vol. 156, pp. 247–259, 2019.
- [19] K. Schild, D. Sutherland, P. Elosegui, and D. Duncan, "Measurements of iceberg melt rates using high-resolution gps and iceberg surface scans," *Geophysical Research Letters*, vol. 48, no. 3, p. e2020GL089765, 2021.
- [20] J. Schönberger and J.-M. Frahm, "Structure-from-motion revisited," in *Conference on Computer Vision and Pattern Recognition (CVPR)*, 2016.
- [21] O. S. McCarthy, M. Winston Pomeroy, and J. E. Smith, "Corals that survive repeated thermal stress show signs of selection and acclimatization," *Plos one*, vol. 19, no. 7, p. e0303779, 2024.
- [22] A. Eltner, L. Bertalan, J. Grundmann, M. T. Perks, and E. Lotsari, "Hydro-morphological mapping of river reaches using videos captured with uas," *Earth Surface Processes and Landforms*, vol. 46, no. 14, pp. 2773–2787, 2021.
- [23] W. T. Tinkham and N. C. Swayze, "Influence of agisoft metashape parameters on uas structure from motion individual tree detection from canopy height models," *Forests*, vol. 12, no. 2, p. 250, 2021.
- [24] B. Mildenhall, P. P. Srinivasan, M. Tancik, J. T. Barron, R. Ramamoorthi, and R. Ng, "Nerf: Representing scenes as neural radiance fields for view synthesis," *Communications of the ACM*, vol. 65, no. 1, pp. 99–106, 2021.
- [25] G. Mazzacca, A. Karami, S. Rigon, E. Farella, P. Trybala, F. Remondino *et al.*, "Nerf for heritage 3d reconstruction," *International Archives of the Photogrammetry, Remote Sensing and Spatial Information Sciences- ISPRS Archives*, vol. 48, no. M-2-2023, pp. 1051–1058, 2023.
- [26] K. Zainuddin, M. Ghazali, F. Marzukhi, A. Samad, M. Mohd Ariff, and Z. Majid, "Evaluation of nerf 3d reconstruction for rock art documentation," *The International Archives of the Photogrammetry, Remote Sensing and Spatial Information Sciences*, vol. 48, pp. 469–475, 2024.
- [27] H. Qichun, X. Haojun, W. Xiaolong, Y. Yizhen, H. Weifeng, H. Xinmin, and L. Caizhi, "Transr-nerf: Super-resolution neural radiance field for reconstruction and rendering of weak and repetitive texture of aviation damaged functional surface," *Chinese Journal of Aeronautics*, 2024.
- [28] A. Murtiyoso, J. Markiewicz, A. Karwel, and P. Kot, "Investigation on the use of nerf for heritage 3d dense reconstruction for interior spaces," *International Archives of the Photogrammetry, Remote Sensing and Spatial Information Sciences- ISPRS Archives*, vol. 48, no. 1/W3-2023, pp. 115–121, 2023.
- [29] H. Vishnu, T. Y. Lin, M. Chitre, B. Kalyan, and E. Venables, "Estimating Floating Ice Coverage in Tidewater Glacier Bays Automatically from Aerial Imagery," in *OCEANS 2024 - Halifax*. IEEE, sep 2024.
- [30] H. Vishnu, M. Chitre, B. Kalyan, T. S. Pieng, D. Stokes, E. Weidner, M. Hoffmann-Kuhnt, and O. Glowacki, "A low-cost surface vehicle for studying the near-terminus region at tidewater glaciers," in *MTS/IEEE OCEANS Conference Brest*, Brest, 2025.
- [31] J. L. Schönberger, E. Zheng, M. Pollefeys, and J.-M. Frahm, "Pixel-wise view selection for unstructured multi-view stereo," in *European Conference on Computer Vision (ECCV)*, 2016.
- [32] Z. Wang, A. C. Bovik, H. R. Sheikh, and E. P. Simoncelli, "Image quality assessment: from error visibility to structural similarity," *IEEE transactions on image processing*, vol. 13, no. 4, pp. 600–612, 2004.
- [33] R. Zhang, P. Isola, A. A. Efros, E. Shechtman, and O. Wang, "The unreasonable effectiveness of deep features as a perceptual metric," in *Proceedings of the IEEE conference on computer vision and pattern recognition*, 2018, pp. 586–595.